ACS APPLIED MATERIALS & INTERFACES

Research Article

www.acsami.org

# Renewable and Superior Thermal-Resistant Cellulose-Based Composite Nonwoven as Lithium-Ion Battery Separator

Jianjun Zhang,[‡,†] Zhihong Liu,[‡,†] Qingshan Kong,[‡] Chuanjian Zhang,[‡] Shuping Pang,[‡] Liping Yue,[§] Xuejiang Wang,[‡] Jianhua Yao,[‡] and Guanglei Cui*[,‡]

[‡]Qingdao Institute of Bioenergy and Bioprocess Technology, Chinese Academy of Sciences, Qingdao 266101, P. R. China

[§]Qingdao University of Science and Technology, Qingdao 266042, P. R. China

Supporting Information

**ABSTRACT:** A renewable and superior thermal-resistant cellulose-based composite nonwoven was explored as lithium-ion battery separator via an electrospinning technique followed by a dip-coating process. It was demonstrated that such nanofibrous composite nonwoven possessed good electrolyte wettability, excellent heat tolerance, and high ionic conductivity. The cells using the composite separator displayed better rate capability and enhanced capacity retention, when compared to those of commercialized polypropylene separator under the same conditions. These fascinating characteristics would endow this renewable composite nonwoven a promising separator for high-power lithium-ion battery.

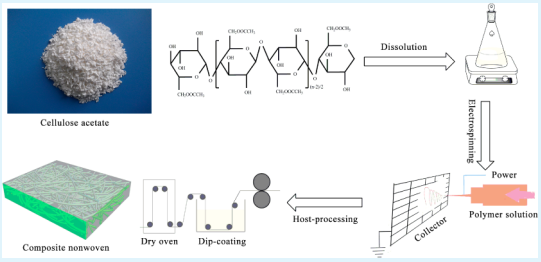


**KEYWORDS:** *cellulose-based composite nonwoven, thermal resistance, renewable, separator, lithium-ion battery*

## INTRODUCTION

lithium-ion battery has drawn extensive attention for portable electronic devices and the emerging fields such as low-emission vehicles and energy storage systems.[1−3] The separator in battery plays an important role in electrically isolating cathode and anode to prevent electrical short circuits and at the same time allow rapid transport of ionic charge carriers. The polyolefin microporous separators such as polyethylene (PE) and polypropylene (PP) membranes are commercially available because of their superior properties such as electrochemical stability, considerable mechanical strength and thermal shut-down property.[4−6] Nevertheless, they have some disadvantages when they are used in future energy storage devices and electric or hybrid-electric vehicles. One of the most serious issues is their inferior thermal stability, due to their low softening or melting temperature.[7] So it is difficult to perform the critical function of electronic isolation between cathode and anode in large-sized batteries at elevated temperature or under vigorous conditions. Tremendous efforts have been made to develop high performance separators with superior electrolyte wettability, improved thermal stability and enhanced rate capability. One strategy was to incorporate inorganic nanoparticles into PE or PP membranes achieving improved thermal and interfacial stability;[8−12] the other one was to fabricate polymeric nonwovens from heat-resistant resins.[13−21] Unfortunately, the incorporation approach suffered from poorly bonded nanoparticles and the nonwovens had a limitation of low mechanical strength.

It is well-known that the polyolefins are not renewable because of their source from the ever-decreasing fossil oil. With exhausted fossil oil and severe environmental pollution, it is obligatory for scientists to find out a sustainable way for the future society. An alternative way to solve this problem is to achieve the transition from fossil-based resources to biomass-based resources. As we all know, cellulose is one of the most abundant, renewable resources on the earth and possesses outstanding properties such as biocompatibility, desired chemical stability and environmental benignancy.[22−28] Furthermore, it was reported that the initial decomposition temperature of cellulose is above 270 °C.[29] These abundance, renewable and superior thermal stability could qualify cellulose a very promising material for battery application instead of fossil-based chemicals. In very recent years, a number of cellulose-based materials have been developed for potential application in lithium-ion battery such as binder, separator and electrolyte additives because of its unique characteristics and providing new greater opportunities.[30−37] Carboxymethyl cellulose (CMC) and natural cellulose were used flexible, porous, low cost and electrochemically stable separator for low power applications.[32] It was also reported that microfibrillated cellulose was utilized to reinforce methacrylic-based polymer electrolyte because of increased Young's modulus, tensile strength, and thermal stability.[35] Furthermore, renewable lignin/conducting polymer interpenetrating networks were also explored as low-cost cathode materials by Inganäs and his co-worker.[37]

So far, there was rare report on renewable cellulose-based nonwoven as high power lithium-ion battery separator owing to

Received: October 11, 2012
Accepted: December 10, 2012
Published: December 10, 2012

  

a poor mechanical property of nonwoven. It is demonstrated that poly(vinylidene fluoride-co-hexafluoropropylene) (PVDF-HPF) is an excellent polymer electrolyte with better anodic stability and good mechanical stability,[38] which is a potential candidate for composite nonwoven. Herein, we presented cellulose/PVDF-HFP composite nonwoven via an electrospinning technique followed by a dip-coating process. It was expected that such renewable cellulose/PVDF-HFP composite separator could possess desirable thermal stability, excellent electrochemical stability and good rate capability. The fascinating characteristics and enhanced battery performance would endow this composite nonwoven a very promising separator for high power application.

## EXPERIMENTAL SECTION

**Preparation of the Cellulose/PVDF-HFP Composite Nonwoven.** Schematic illustration for the renewable cellulose-based composite separator preparation was shown in Scheme 1. The

**Scheme 1. Schematic Illustration for the Renewable Cellulose-Based Composite Separator Preparation**

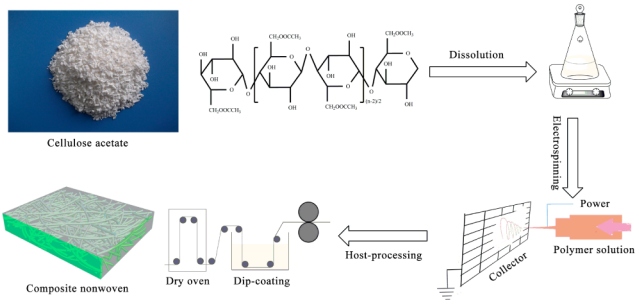


cellulose acetate solution was prepared at room temperature by dissolving the cellulose acetate in (v/v) 2:1 DMAc/acetone mixture solvent at a concentration of 15% w/w. The cellulose acetate solution was electrospun at a positive voltage of 27 kV, a tip-to-collector distance of 15 cm, and a solution flow rate of 2 mL/h. The obtained cellulose acetate membrane was detached from the collector and dried under vacuum at 70 °C for 8 h. Hydrolysis of cellulose acetate membrane was performed in 0.05 M LiOH aqueous ethanol solutions at ambient temperature for 12 h. Then the obtained membrane was rinsed in distilled water and dried under vacuum at 80 °C for 10 h.

The solution for coating layers was composed of PVDF-HFP and acetone, wherein the ratio of PVDF-HFP/acetone was fixed at 2/98 (wt %/wt %). The cellulose nonwoven was soaked in the coating solution by a dip-coating process. The PVDF-HFP solution-immersed cellulose nonwoven was then dried at 80 °C in vacuum to remove acetone. Hot calendering was further carried out, which temperature and pressure was set to 100 °C and 5 MPa, respectively. The final thickness of cellulose/PVDF-HFP composite nonwoven was 27 $\mu$m.

**Materials Characterization.** The surface morphology of separators was observed by a Hitachi S-4800 field emission scanning electron microscope (SEM). The pore size measurement of separators was measured by a ASAP 2020-M+C porosimeter. The porosity of the separator was determined using n-butanol uptake method. For this purpose, the mass of the separator was measured before and after immersion in n-butanol for 2 h. The porosity of the membrane was calculated using the equation: porosity=$(m_b/\rho_b)/(m_b/\rho_b + m_p/\rho_p) \times 100\%$, where $m_b$ and $m_p$ are the mass of n-butanol and the separator, $\rho_b$ and $\rho_p$ are the density of n-butanol and the separator, respectively. For example, we used density of PP to calculate the porosity of PP separator. Meanwhile we used density of cellulose to calculate the porosity of cellulose nonwoven. The air permeability of the separator was examined with a Gurley densometer (4110N, Gurley) by measuring the time for air to pass through a determined volume (100 cc). The electrolyte uptake was obtained by measuring the weight of separator before and after soaking in liquid electrolyte for 2 h and then calculated using following equation. Electrolyte uptake = $(W_f - W_i)/W_i \times 100\%$, where $W_i$ and $W_f$ are the weight of the separator before and after soaking in the liquid electrolyte, respectively. Contact angle measurements were performed using a JC2000C goniometer. Contact angles were measured using 5 $\mu$L electrolyte droplets. The chemical structure of the membranes was characterized by Fourier transform infrared spectroscopy (FT-IR, Bruker VERTEX 70). The mechanical property was measured using an Inston-3300 universal testing machine (USA) at a stretching speed of 1.66 mm sec$^{-1}$ with the sample straps of about 1 cm wide and 8 cm long. The experiment on mechanical properties was carried out for four times. To evaluate its thermal shrinkage behavior, the separator was placed in an oven and heated at 200 °C for 0.5 h. Thermal stability of the separator was examined by a differential scanning calorimeter (Diamond DSC, PerkinElmer) ranging from 50 to 300 °C at 10 °C min$^{-1}$ under a $N_2$ atmosphere.

**Electrochemical Measurements.** For measurement of electrochemical performance, a liquid electrolyte of 1 M $LiPF_6$ in EC/DMC (1/1, v/v) was employed. The electrochemical stability window of the separator was determined by a linear sweep voltammetry experiment performed on a working electrode of stainless-steel and a counter electrode of lithium metal at a scan rate of 1.0 mV s$^{-1}$. The ionic conductivity of the liquid electrolyte-soaked separator between two stainless-steel plate electrodes, the interfacial resistances between liquid electrolyte-soaked separator and lithium metal electrodes and AC impedance measurement of the cells were evaluated using the electrochemical impedance spectroscopy (EIS) measurement by applying an AC voltage of 20 mV amplitude in the frequency range of 1 to $1 \times 10^6$ Hz.

A unit cell (2032-type coin) was assembled by sandwiching a separator between a $LiCoO_2$ cathode ($LiCoO_2$/carbon black/PVDF 90/5/5 w/w/w) and a natural graphite anode (natural graphite/carbon black/CMC/SBR 93/5/1.25/0.75 w/w/w/w), and then activated by filling it with the liquid electrolyte of 1 M $LiPF_6$/EC +DMC (1:1, v/v). All assembly of cells was carried out in an argon-filled glovebox. For comparison, cells using the PP separator (Celgard 2500) were assembled and tested under the same condition. The discharge current densities were varied from 0.2 to 8.0 C under a voltage range between 2.75 and 4.2 V. The cells were cycled at a fixed charge/discharge current density of 0.5 C/0.5 C for cycle life testing.

## RESULTS AND DISCUSSION

Figure 1a–d showed typical SEM images of the nanofibrous cellulose nonwoven and the cellulose/PVDF-HFP composite nonwoven, respectively. It was observed in a and b in Figure 1 that the cellulose nonwoven consisted of randomly arranged

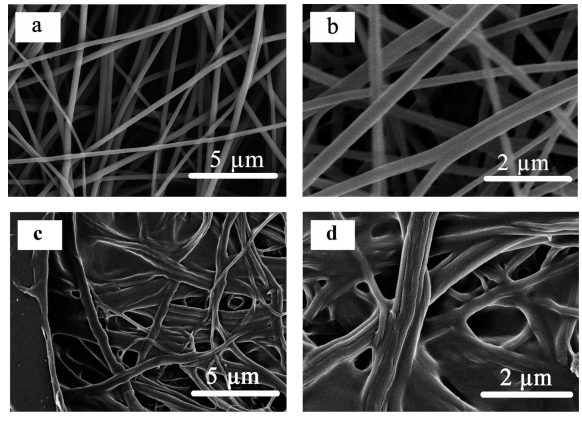


**Figure 1.** Typical SEM image and its enlarged image of the (a, b) cellulose nonwoven and (c, d) cellulose/PVDF-HFP composite nonwoven.


dx.doi.org/10.1021/am302290n | ACS Appl. Mater. Interfaces 2013, 5, 128–134

nanofibers with an average diameter size of 300 nm and it possessed excessively large-sized pores (>2 $\mu$m), which was not beneficial to maintain the battery voltage due to self-discharge and also vulnerable to breakdown at high discharge rates or under vigorous conditions. It was demonstrated in Figure 1c, d that PVDF-HFP had been incorporated between the cellulose nanofibers and the nonwoven showed smaller pore sizes. From Figure S1 in the Supporting Information, it can be found that the pore size distribution of the cellulose/PVDF-HFP composite nonwoven was discontinuous. Most of its pore dimensions were less than 100 nm, thus confirming that cellulose/PVDF-HFP composite nonwoven possessed uniform pore distribution. These tortuous small pores and uniform pore size distribution were expected to play a key role in mitigating self-discharge and achieving uniform current density at high charge/discharge rates, which was advantageous to prevent formation of lithium dendrites.

The thickness, porosity, air permeability, and electrolyte uptake of the PP separator and the cellulose-based separators were listed in Table 1. The Gurley value of the cellulose/PVDF-HFP composite nonwoven was 32.7 s, which was much lower than that of the PP separator (235 s),[12] although it was higher than that of pristine cellulose nonwoven (6.6 s). It is well-known that highly porous structure of separator gave rise to lower Gurley value.[19] The improvement in the microporous structure of the nonwoven was further confirmed by the porosity data of the separators. It is worth noticing that the porosity of the cellulose/PVDF-HFP nonwoven (65%) was fairly higher than that of PP separator (55%) and lower than that of cellulose nonwoven (75%). It was deduced that although PVDF-HFP coating alleviated the porosity of cellulose nonwoven, the composite nonwoven still possessed considerable porosity for holding sufficient liquid electrolyte in facilitating rapid ionic transportation.

**Table 1. Physical Properties of the Cellulose-Based Separators**

| sample | thickness ($\mu$m) | porosity (%) | Gurley value (s) | Gurley value (200 °C) (s) | electrolyte uptake (%) |
|---|---|---|---|---|---|
| PP separator[a] | 25 | 55 | 235 | | 120 |
| cellulose nonwoven | 25 | 75 | 6.6 | 6.6 | 340 |
| cellulose/PVDF-HFP | 27 | 65 | 32.7 | 36 | 280 |

[a]PP separator is melted at 165 °C.

The electrolyte wettability of separators was crucial for cycle performance of lithium-ion battery. The electrolyte wettability of the PP separator and the cellulose/PVDF-HFP composite nonwoven was vividly shown in Figure 2. The wettability of PP separator with electrolyte was poor, because of its hydrophobic surface characteristic and low surface energy.[39] In contrast, the cellulose/PVDF-HFP composite nonwoven could be rapidly wetted by the liquid electrolyte and its electrolyte uptake became saturated within 5 s, which was indicative of better affinity between the cellulose/PVDF-HFP composite nonwoven and the electrolyte. This superior liquid electrolyte wettability may be attributed to the unique chemical structure of the cellulose and the porous structure of the nanofiberous nonwoven. In addition, although the electrolyte uptake of

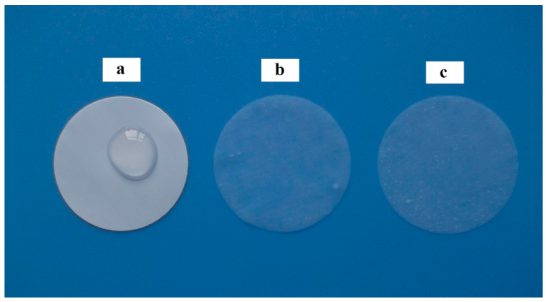


**Figure 2.** Photograph showing liquid electrolyte wettability of the (a) PP separator, (b) cellulose nonwoven, and (c) cellulose/PVDF-HFP composite nonwoven.

cellulose/PVDF-HFP composite nonwoven (280%) was lower than that of cellulose nonwoven, it was still four times as much as that of PP separator (60%).[6]

In addition, contact angle measurements with electrolyte droplets (1 M $LiPF_6$ in EC/DMC) were also conducted to investigate the surface properties of the PP separator and the cellulose/PVDF-HFP composite nonwoven. As shown in Figure S2 in the Supporting Information, the contact angle of PP separator (103°) was much higher than that of cellulose/PVDF-HFP composite nonwoven (55°) and, thus, confirmed that cellulose/PVDF-HFP composite nonwoven possessed better wettability compared to the bare PP separator. In most cases, composite nonwoven readily absorbed the liquid electrolyte, which showed that there were a good affinity between electrolyte and separators and therefore had a good capability of retaining the electrolyte solutions within the separators. Thus, high porosity, lower Gurley value, and superior wettability of cellulose/PVDF-HFP composite nonwoven were beneficial to improve the rate capability and cycle performance of lithium-ion battery.

To evaluate the thermal properties, we conducted DSC measurements on the PP separator and cellulose/PVDF-HFP composite nonwoven (shown in Figure 3). It was observed in Figure 3 that the PP separator had an endothermic peak appearing at 165 °C relating to its melting point. And the cellulose/PVDF-HFP composite nonwoven did not show any obvious endothermic peak below 300 °C, which implied that the cellulose/PVDF-HFP composite nonwoven possessed better thermal stability than PP separator. It was reported that the bulky PVDF-HFP possessed a melting point at about 145 °C;[40] however, in our case, the minimal amount of

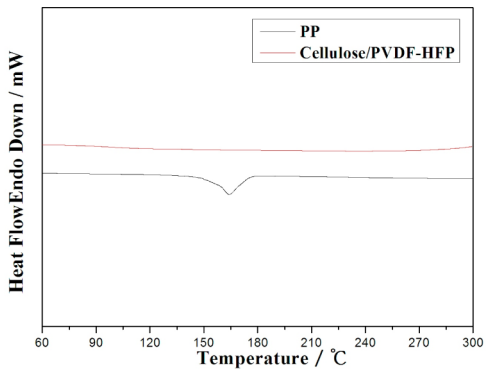


**Figure 3.** DSC curves of the PP separator and cellulose/PVDF-HFP composite nonwoven.


dx.doi.org/10.1021/am302290n | ACS Appl. Mater. Interfaces 2013, 5, 128−134

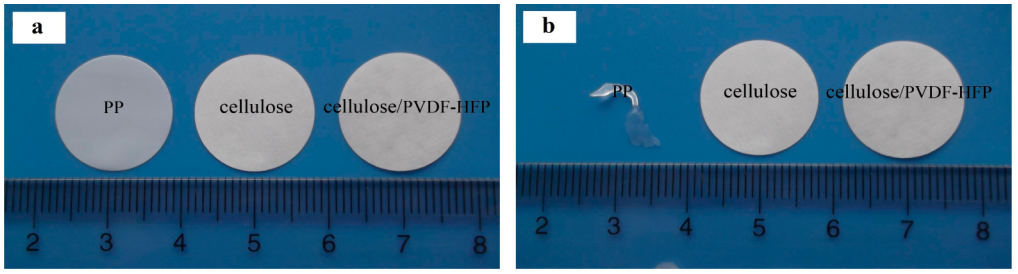


**Figure 4.** Photographs of PP separator, cellulose nonwoven, and cellulose/PVDF-HFP composite nonwoven (a) before and (b) after thermal treatment at 200 °C for 0.5 h.

incorporated PVDF-HFP (3 wt %) could not contributed to an obvious endothermic peak.

Thermal shrinkage of separators is another concern on battery safety characteristic.[41−43] Figure 4 showed the photographs of the separators after they were thermally treated in oven at 200 °C for 0.5 h. The cellulose/PVDF-HFP composite nonwoven exhibited negligible dimension change, whereas PP separator melt down and shrank by 90%. Furthermore, Gurley value of the separators at an elevated temperature of 200 °C was presented in Table 1. Apparently, Gurley value of PP separator could not be determined as PP separator melted at 165 °C. On the contrary, Gurley value of cellulose/PVDF-HFP composite nonwoven at 200 °C was 36 s, which was similar to that of cellulose/PVDF-HFP composite nonwoven at room temperature. This superior thermal tolerance could effectively prevent internal electrical short circuit at elevated temperature when the battery was at high charged/discharged rates. Therefore, cellulose-based composite nonwoven has great potential application in a high-temperature condition.[44]

The stress−strain curves of the cellulose/PVDF-HFP composite nonwoven in dry and wet states are depicted in Figure 5. Brief mechanical parameters of PP separator and

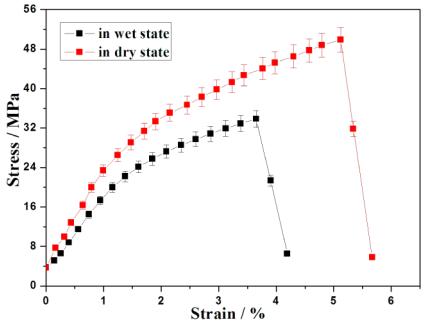


**Figure 5.** Stress−strain curves of the cellulose/PVDF-HFP composite nonwoven in dry and wet states.

cellulose/PVDF-HFP composite nonwoven were listed in Table S1 in the Supporting Information. Apparently, the maximum stress was 50 MPa and the deformation was 5.2% in dry state. It was also found that the cellulose/PVDF-HFP composite nonwoven after being soaked in the liquid electrolyte for 2 h exhibited reduced tensile strength of 33 MPa and deformation of 3.5%. It was obvious that the tensile strength of the cellulose/PVDF-HFP composite nonwoven was much better than the transverse strength of the commercial PP separator (12 MPa) and lower than that of PP separator at the machine direction (120 MPa).[11] Interestingly, the cellulose/PVDF-HFP composite nonwoven has a considerably higher Young's modulus (960 MPa) than that of the PP separator (240 MPa). This feature of high Young's modulus is advantageous to remain mechanical integrity for the separator when it encounters accident collision. In regards of safety issue, the robust cellulose/PVDF-HFP composite nonwoven will deliver more reliable mechanical property and avoid the rupture of the separator.

To investigate the chemical inert of cellulose/PVDF-HFP composite nonwoven, we have presented the accelerated experiment to characterize chemical stability with electrolyte which was composed of 1 M $LiPF_6$ in EC/DMC (1/1, v/v), Figure S3 in the Supporting Information. showed FTIR data of cellulose/PVDF-HFP composite nonwoven before and after immerse in electrolyte at 50 °C for 2 weeks. As shown in Figure S3 in the Supporting Information, although cellulose/PVDF-HFP composite nonwoven was dipped in electrolyte at 50 °C for 2 weeks, FTIR data of cellulose/PVDF-HFP composite nonwoven maintained the chemical structure well, thus proving cellulose/PVDF-HFP composite nonwoven was chemically stable comparable to that of PP separator in electrolyte.

The interfacial compatibility of lithium metal with separator plays an important role in lithium batteries for practical application. Figure 6 depicted the interfacial compatibility of

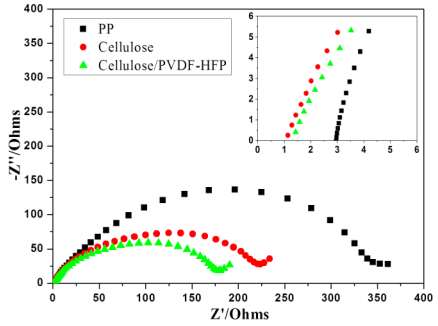


**Figure 6.** Nyquist plots of Li/electrolyte-soaked separator/Li cells at 30 °C.

the liquid electrolyte-soaked separators with a lithium metal anode, which was characterized by the electrochemical impedance spectroscopy. It could be observed that the interfacial resistance was 180 Ω for the cellulose/PVDF-HFP composite nonwoven, 227 Ω for the cellulose nonwoven, and 340 Ω for the PP separator. Obviously, a lower interfacial resistance between lithium metal and separator could be obtained in the case of cellulose/PVDF-HFP composite nonwoven, which indicated that cellulose/PVDF-HFP composite nonwoven could endow better interfacial characteristics for lithium-ion battery separator.

For practical battery applications, it is important to investigate the electrochemical stability of the electrolytes


dx.doi.org/10.1021/am302290n | ACS Appl. Mater. Interfaces 2013, 5, 128−134

within the operation voltage of the battery system. Electrochemical stability, an important issue in characterizing battery separators, was examined by the linear sweep voltammograms on a stainless steel electrode as a working electrode with lithium as a reference electrode. Figure 7 displayed the linear sweep

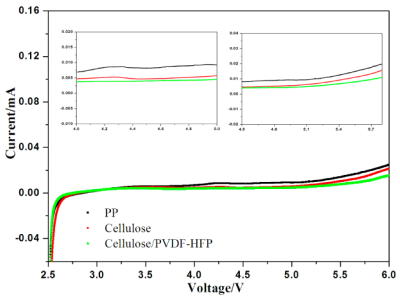


**Figure 7.** Linear sweep voltammograms of the PP separator, cellulose nonwoven, and cellulose/PVDF-HFP composite nonwoven at a scan rate of 1.0 mV $s^{-1}$. The inset (top left) shows the region (4.5−5.8 V) and the inset (top right) shows the region (4.0−5.0 V).

voltammograms of the PP separator, cellulose nonwoven and cellulose/PVDF-HFP composite nonwoven. There was a hump at about 4.2 V vs $Li^+$/Li in the electrolyte soaked PP separator and cellulose nonwoven, which could be ascribed to trace water in the commercial electrolyte. And no obvious hump was observed in the electrolyte soaked cellulose/PVDF-HFP composite nonwoven for super hydrophobicity of PVDF-HFP suppressed the contact of water with interface electrode.[45] It was also observed in Figure 7 that the electrolyte with PP separator, cellulose nonwoven and cellulose/PVDF-HFP composite nonwoven decomposed at about 4.8, 5.0, and 5.3 V, respectively. Obviously, electrolyte based on the cellulose/PVDF-HFP composite nonwoven exhibited best anodic stability. This could be ascribed to the better electrolyte retention and superior interfacial compatibility of the composite separator. It was noted that the electrolyte soaking in cellulose/PVDF-HFP composite nonwoven displayed better electrochemical stability than that of cellulose nonwoven, due to compositing with the high electrochemical stability of PVDF-HFP material. It is a common sense that carbonate electrolytes possess a decomposition voltage around 4.5 V vs $Li^+$/Li.[46] In our case, no obvious decomposition of carbonate electrolytes occurred below 5 V vs $Li^+$/Li using cellulose/PVDF-HFP nonwoven as separator. These results suggest that the composite nonwoven is very promising for applications in high energy lithium-ion battery.

Figure 8 depicted Arrhenius plots of ionic conductivity of liquid electrolyte-soaked PP separator, cellulose nonwoven and cellulose/PVDF-HFP composite nonwoven. At 30 °C, the obtained ionic conductivity was 0.64, 1.75, and 1.04 mS $cm^{-1}$ for PP separator, cellulose nonwoven, and cellulose/PVDF-HFP composite nonwoven, respectively. The difference in ionic conductivity could be ascribed to the electrolyte uptake from the different porosity. Considering a considerable porosity, the ionic conductivity of liquid electrolyte-soaked cellulose/PVDF-HFP composite nonwoven was higher than that of PP separator mainly because of the excellent composite structure. The ionic conductivity of liquid electrolyte-soaked cellulose nonwoven was superior to that of cellulose-based composite nonwoven owing to a better porosity. Taking into account other factors, such as physical property, electrochemical, and interfacial

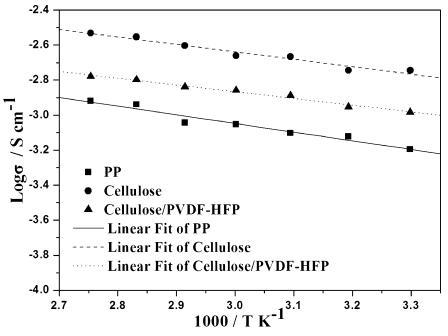


**Figure 8.** Arrhenius plots of ionic conductivity of liquid electrolyte-soaked PP separator, cellulose nonwoven, and cellulose/PVDF-HFP composite nonwoven.

stability, cellulose-based composite nonwoven would be more beneficial to the performance of the cells.[47]

The cell performance of the PP separator and cellulose/PVDF-HFP composite separator, including discharge capacity, discharge *C*-rate capability, and cycle performance at various charge/discharge conditions, were investigated. Figure 9

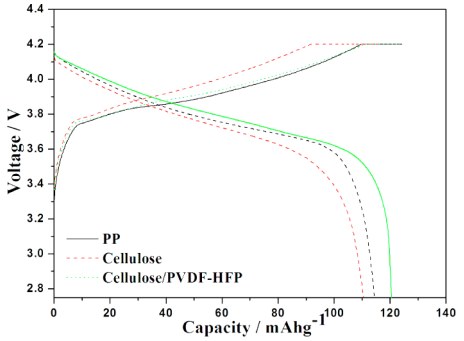


**Figure 9.** Charge/discharge curves for the cells using the PP separator, cellulose nonwoven and cellulose/PVDF-HFP composite separator at 0.5 *C* rate. (1 *C* = 130 mA $g^{-1}$).

presented the typical voltage-specific capacity curves at a rate of 0.5 C for the cells using the PP separator, cellulose nonwoven and the cellulose/PVDF-HFP composite separator. The discharge capacities of the PP separator and the cellulose/PVDF-HFP composite separator were comparable, about 118 and 120 mA h $g^{-1}$ at 0.5 C, respectively. The stable voltage profiles would be partly ascribed to the electrochemical interfacial stability of the cellulose/PVDF-HFP composite separator. Moreover, the initial discharge voltage were comparable, 4.15 and 4.16 V for PP separator and cellulose/PVDF-HFP composite separator, respectively, which was higher than that of cellulose nonwoven (4.12 V). This probably ascribed to the self-discharge phenomenon of cellulose nonwoven, owing to large-sized pores of the nonwoven that were not beneficial to maintain stable open voltage of the battery. So such cellulose-based composite nonwoven was a good candidate separator for high-performance lithium-ion battery.

In addition, the cells with the cellulose/PVDF-HFP composite separator exhibited much better rate capability as compared to the PP separator at various rates (Figure 10). For example, the cellulose/PVDF-HFP composite separator kept a specific capacity of 118 mA h $g^{-1}$ at 0.5 *C*, whereas the specific capacity of the PP separator was 112 mA h $g^{-1}$. The specific


dx.doi.org/10.1021/am302290n | *ACS Appl. Mater. Interfaces* 2013, 5, 128−134

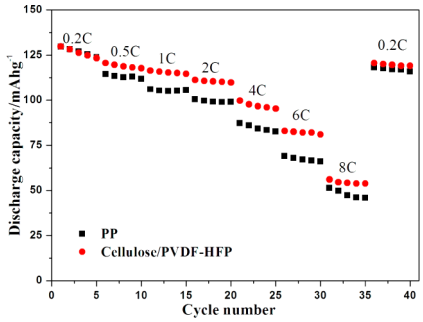


**Figure 10.** Rate capability of the cells using PP separator and cellulose/PVDF-HFP composite separator.

capacity of the cells using the cellulose/PVDF-HFP composite separator and PP separator at other various rates was 115 and 106 mA h $g^{-1}$ at 1.0 *C*, 110 and 99 mA h $g^{-1}$ at 2.0 *C*, 96 and 83 mA h $g^{-1}$ at 4.0 *C*, 82 and 63 mA h $g^{-1}$ at 6.0 *C*, 54 and 46 mA h $g^{-1}$ at 8.0 C, respectively. It was very interesting that when the rate returned to 0.2 *C* after the rate test, the reversible capacity of the cells with PP separator and cellulose/PVDF-HFP composite nonwoven were 118 and 121 mA h $g^{-1}$, respectively, which were very close to the original capacity. The Celgard 2500 was ever reported to exhibit the best rate capability among the Celgard separators.[48] In our case, the composite separator possessed better rate capability than the Celgard 2500. The enhanced rate capability was ascribed to lower interfacial resistance and higher ionic conductivity of the electrolyte-soaked cellulose/PVDF-HFP composite separator.

It was depicted in Figure 11 that the discharge capacities as a function of cycle number (up to 100 cycles) of the cellulose/

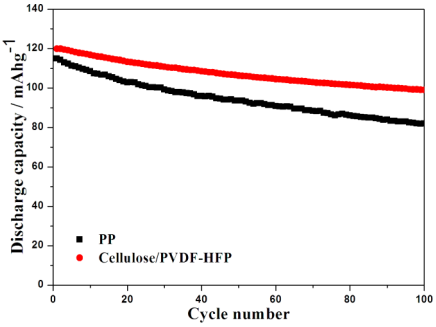


**Figure 11.** Cycle performance of the cells using PP separator and cellulose/PVDF-HFP composite separator.

PVDF-HFP composite separator and PP separator at charge/discharge rate of 0.5 C. The obtained discharge capacity after 100 cycles was around 99 mA h $g^{-1}$ indicative of capacity retention at 83% better than 71% of the PP separator. This superior cycle performance of the cellulose/PVDF-HFP composite separator would be attributed to better liquid electrolyte retention and electrochemically interfacial stability.

To understand the variation of cell impedances during cycle test, AC impedance measurement was carried out for the cells after the first cycle and after the 50 cycles test. The semicircle represents the charge-transfer resistance, accompanied with migration of lithium ion at the electrode/electrolyte interface. The straight slopping line corresponds to the diffusion of lithium ion in the active material of electrode.[49] As shown in Figure S4a in the Supporting Information, the charge-transfer resistance of cellulose/PVDF-HFP nonwoven after first cycle was 15 Ω, which slightly lower to that (16 Ω) of PP separator. However, obvious differences of the charge transfer regime after 50 cycles were observed in Figure S4b in the Supporting Information. Obviously, the charge-transfer resistance of cellulose/PVDF-HFP composite nonwoven was 21 Ω, whereas that of the PP separator displayed 50 Ω. The difference of charge-transfer resistance between the PP separator and the cellulose/PVDF-HFP nonwoven directly related to a favorable interface and increased retention of the liquid electrolyte in cellulose/PVDF-HFP composite nonwoven.[50] The better rate capability and cycling performance of the cell with cellulose/PVDF-HFP than that with PP separator would be understand in terms of lower resistance of cellulose/PVDF-HFP composite nonwoven.

## CONCLUSIONS

In this paper, we presented a renewable, low cost, and environmentally benign cellulose/PVDF-HFP composite nonwoven as an advanced separator for high-performance lithium-ion battery. Compared to the commercialized PP separator, the cellulose/PVDF-HFP composite separator possessed not only higher ionic conductivity and better electrolyte uptake but also superior thermal resistance and enhanced electrochemically interfacial stability. It was demonstrated that the batteries using the composite nonwoven separator exhibited much better rate capability, higher discharge capacity and superior capacity retention. Thus, the renewable cellulose/PVDF-HFP composite nonwoven should be very promising candidate separator for high-power lithium-ion battery.

## ASSOCIATED CONTENT

### Supporting Information

Pore distribution, contact angle images, FTIR data, Nyquist plots, and mechanical properties. This material is available free of charge via the Internet at http://pubs.acs.org.

## AUTHOR INFORMATION

### Corresponding Author

*Fax: +86 532 80662744. E-mail: cuigl@qibebt.ac.cn.

### Author Contributions

†These authors contributed equally to this work.

### Notes

The authors declare no competing financial interest.

## ACKNOWLEDGMENTS

This work was supported by the National Program on Key Basic Research Project of China (973 Program) (MOST2011CB935700), the Instrument Developing Project of the Chinese Academy of Sciences (YZ201137), the"100 Talents" program of the Chinese Academy of Sciences.

## REFERENCES

(1) Li, H.; Wang, Z.; Chen, L.; Zhang, X. *Adv. Mater.* **2009**, *21*, 4593−4607.
(2) Hassoun, J.; Panero, S.; Reale, P.; Scrosati, B. *Adv. Mater.* **2009**, *21*, 4807−4810.
(3) Palacin, M. R. *Chem. Soc. Rev.* **2009**, *38*, 2565−2575.
(4) Venugopal, G.; Moore, J.; Howard, J.; Pendalwar, S. *J. Power Sources* **1999**, *77*, 34−41.
(5) Arora, P.; Zhang, Z. *Chem. Rev.* **2004**, *104*, 4419−4462.
(6) Zhang, S. S. *J. Power Sources* **2007**, *164*, 351−364.
(7) Huang, X. S. *J. Solid State Electrochem.* **2011**, *15*, 649−662.
(8) Jeong, H. S.; Lee, S. Y. *J. Power Sources* **2011**, *196*, 6716−6722.

(9) Choi, J. A.; Kim, S. H.; Kim, D. W. *J. Power Sources* **2010**, *195*, 6192−6196.
(10) Park, J. H.; Cho, J. H.; Park, W.; Ryoo, D.; Yoon, S. J.; Kim, J. H.; Jeong, Y. U.; Lee, S. Y. *J. Power Sources* **2010**, *195*, 8307−8312.
(11) Jung, H. R.; Ju, D. H.; Lee, W. J.; Zhang, X.; Kotek, R. *Electrochim. Acta* **2009**, *54*, 3630−3637.
(12) Fu, D.; Luana, B.; Steve, M.; Bureau, A.; Isobel, D. J. *J. Power Sources* **2012**, *206*, 328−334.
(13) Fausto, C.; Focarete, M. L.; Hassoun, J.; Meschinia, A. J.; Scrosati, B. *Energy Environ. Sci.* **2011**, *4*, 921−927.
(14) Carol, P.; Ramakrishnan, P.; John, B.; Cheruvally, G. *J. Power Sources* **2011**, *196*, 10159−10169.
(15) Jeong, H. S.; Choi, S.; Kim, J. H.; Lee, S. Y. *Electrochim. Acta* **2011**, *56*, 5202−5213.
(16) Jeong, H. S.; Noh, J. H.; Hwang, C. G.; Kim, S. H.; Lee, S. Y. *Macromol, Chem. Phys.* **2010**, *211*, 420−425.
(17) Jeong, H. S.; Kim, J. H.; Lee, S. Y. *J. Mater. Chem.* **2010**, *20*, 9180−9186.
(18) Yang, C.; Liu, Z.; Wang, Z.; Wang, L. *J. Power Sources* **2009**, *189*, 716−718.
(19) Cho, T. H. E.; Tanaka, M.; Ohnishi, H.; Kondo, Y.; Yoshikawa, M.; Nakamura, T.; Sakai, T. *J. Power Sources* **2010**, *195*, 4272−4276.
(20) Qi, W.; Lu, C.; Chen, P.; Han, L.; Yu, Q.; Xu, R. Q. *Mater. Lett.* **2012**, *66*, 240−242.
(21) Chun, S. J.; Choi, E. S.; Lee, E. H.; Kim, J. H.; Lee, S. Y.; Lee, S. Y. *J. Mater. Chem.* **2012**, *22*, 16618−16626.
(22) Cherian, B. M.; Leao, A. L.; Souza, S. F.; Manzine Costa, L. M.; Oliveira, G. M.; Kottaisamy, M.; Nagarajan, E. R.; Thomas, S. *Carbohydr. Polym.* **2011**, *86*, 1790−1798.
(23) Chen, S. W.; Ma, X.; Wang, M. R. *J. Biotechnol.* **2008**, *136*, S419−S420.
(24) Edgar, K. J.; Buchanan, C. M.; Debenham, J. S.; Rundquist, P. A.; Seiler, B. D.; Shelton, M. C.; Tindall, D. *Prog. Polym. Sci.* **2001**, *26*, 1605−1688.
(25) Wang, Z. H.; Chien, W. C.; Liu, T. W.; Wang, S. C. *J. Membr. Sci.* **2008**, *310*, 141−148.
(26) Reddy, N.; Wang, Q. *Bioresour. Technol.* **2009**, *100*, 3563−3569.
(27) Jackson, E. L.; Hudson, C. S. *J. Am. Chem. Soc.* **1937**, *59*, 2049−2050.
(28) Zhou, L.; He, J.; Zhang, J.; He, Z.; Hu, Y.; Zhang, C. B.; He, H. *J. Phys. Chem. C* **2011**, *115*, 16873−16878.
(29) Liu, H. Q.; Hsieh, Y. L. *J. Polym. Sci. Phys.* **2002**, *40*, 2119−2129.
(30) Jeong, S. S.; Böckenfeld, N.; Balducci, A.; Winters, M. *J. Power Sources* **2012**, *199*, 331−335.
(31) Li, J.; Klöpsch, R.; Nowak, S.; Kunze, M.; Winter, M.; Passerini, S. *J. Power Sources* **2011**, *196*, 7687−7691.
(32) Zhang, L. C.; Sun, X.; Hu, Z.; Yuan, C. C.; Chen, C. H. *J. Power Sources* **2012**, *204*, 149−154.
(33) Lewis, H.; Grant, C.; Salkind, A. *J. Power Sources* **1997**, *65*, 29−38.
(34) Kuribayashi, I. *J. Power Sources* **1996**, *63*, 87−91.
(35) Chiappone, A.; Nair., J. R.; Gerbaldi, C.; Jabbour, L.; Bongiovanni, R.; Zeno, E.; Beneventi, D.; Penazzi, N. *J. Power Sources* **2011**, *196*, 10280−10288.
(36) Chelmecki, M.; Meyer, W. H.; Wegner, G. *J. Appl. Polym. Sci.* **2007**, *105*, 25−29.
(37) Milczarek, G.; Inganäs, O. *Science* **2012**, *335*, 1468−1471.
(38) Stephan, A. M.; Teeters, D. *J. Power Sources* **2003**, *119*, 460−464.
(39) Ryou, M. H.; Lee, Y. M.; Park, J. K.; Choi, J. W. *Adv. Mater.* **2011**, *23*, 3066−3070.
(40) Ji, G. L.; Xu, Y. Y.; Zhu, B. K.; Zhu, L. P. *J Macromol. Sci. B* **2011**, *50*, 275−290.
(41) Song, J. C.; Ryou, M. H.; Son, B.; Lee, J. N.; Lee, D. J.; Lee, Y. M.; Choi, J. W.; Park, J. K. *Electrochim. Acta* **2012**, *85*, 524−530.
(42) Cho, T. H.; Tanaka, M.; Ohnishi, H.; Kondo, Y.; Yoshikazu, M.; Nakamura, T.; Sakai, T. *J. Power Sources* **2010**, *195*, 4272−4277.
(43) Miao, Y. E.; Zhu, G. N.; Hou, H. Q.; Xia, Y. Y.; Liu, T. X. *J. Power Sources* **2013**, *226*, 82−86.
(44) Mestre, A. F.; Hamelet, S.; Masquelier, C.; Palacin, M. R. *J. Power Sources* **2010**, *195*, 6897−6901.
(45) Liu, K. S.; Yao, X.; Jiang, L. *Chem. Soc. Rev.* **2010**, *39*, 3240−3255.
(46) Xu, K. *Chem. Rev.* **2004**, *104*, 4303−4418.
(47) Djian, D.; Alloin, F.; Martinet, S.; Lignier, H. J.; Sanchez, Y. *J. Power Sources* **2007**, *172*, 416−421.
(48) Jeong, H. S.; Kim, D. W.; Jeong, Y. U.; Lee, S. Y. *J. Power Sources* **2010**, *195*, 6116−6120.
(49) Lee, Y. S.; Jeong, Y. B.; Kim, D. W. *J. Power Sources* **2010**, *195*, 6197−6201.
(50) Gao, K.; Hu, X.; Yi, T.; Dai, C. *Electrochim. Acta* **2006**, *52*, 443−449.